Journal of Magnetic Resonance **145,** 73–83 (2000)
doi:10.1006/jmre.2000.2065, available online at http://www.idealibrary.com on IDEAL®

Compound Radiofrequency-Driven Recoupling Pulse Sequences for Efficient Magnetization Transfer by Homonuclear Dipolar Interaction under Magic-Angle Spinning Conditions

Toshimichi Fujiwara, Purnima Khandelwal,[1] and Hideo Akutsu

Department of Chemistry and Biotechnology, Faculty of Engineering, Yokohama National University, 79-5 Tokiwadai, Hodogaya-ku, Yokohama 240-8501, Japan

E-mail: tfjwr@ynu.ac.jp

Received September 30, 1999; revised February 29, 2000

The maximum of the transferred magnetization in rotating powdered solids under the radiofrequency-driven recoupling (RFDR) pulse sequence is enhanced by reducing the orientation dependence of the effective recoupled homonuclear dipolar interaction. The compound RFDR (CRFDR) pulse sequence for this enhancement consists of RFDR pulse units (τ_i–π–τ_R–π–$\bar{\tau}_i$) with different τ_i, where τ_R is the sample rotation period, τ_i and $\bar{\tau}_i$ ($=\tau_R - \tau_i$) are delays, and π is a 180° pulse. The delay τ_i modifies the zero-quantum spin operators and the sample rotation-angle dependence of the recoupled dipolar Hamiltonian. The CRFDR pulse sequences were optimized for mixing by varying τ_i. Numerical simulation for the two-spin system only with a dipolar interaction and isotropic chemical shifts indicates that the transfer efficiency of CRFDR averaged over the powder is about 70%, which is 30% higher than the efficiency of the RFDR pulse over a broad range of about $1/\tau_R$ in resonance frequency difference. The CRFDR sequences need about 60% longer mixing times to maximize the transferred magnetizaion in comparison with the original RFDR sequence. Chemical shift anisotropy, the other dipolar interactions, and relaxation generally reduce the enhancement by CRFDR. Experiments for fully ^{13}C-labeled alanine, however, show that the maximum of the magnetization transferred with CRFDR from the carboxyl to α carbon is about 15% greater than that with RFDR.

Key Words: **magic-angle spinning; magnetization transfer; solid-state NMR; recoupling; homonuclear dipolar interaction.**

INTRODUCTION

A number of methods for recoupling homonuclear dipolar interactions under magic-angle spinning (MAS) conditions have been proposed during the past decade (*1–3*). These methods, such as rotation-synchronized RF pulse sequences, reintroduce the dipolar Hamiltonian, which contains the zero- or double-quantum spin operators. The recoupled dipolar interactions enable the magnetization transfer (*4–7*) and the measurement of dipolar coupling constants, i.e., internuclear distances (*8–11*). This magnetization transfer under MAS conditions has been utilized for the mixing period in multidimensional correlation NMR experiments for distance and torsion angle measurements (*12–16*), and signal assignments (*17–19*) over broadbands.

The pulse sequences C7 (*20*), POST-C7 (*21*), CMR7 (*22*), and SPC-5 (*23*) originating from the HORROR experiment (*24*) yield the dipolar interactions having double-quantum (DQ) spin operators under MAS conditions, and are shown to be efficient for the broadband magnetization transfer, DQ filter, and torsion angle measurements (*25*). These methods eliminate the orientation dependence of the dipolar interactions on γ, the rotation angle about the sample spinning axis, so that they improve the theoretical magnetization transfer efficiency up to 73%.

In this paper, we describe the improvement of broadband magnetization transfer by the zero-quantum (ZQ) dipolar interaction recovered with the radiofrequency-driven recoupling (RFDR) pulse sequence (*26–32*). The RFDR pulse sequence is a π pulse train with the pulse intervals of the sample spinning period τ_R. This RFDR pulse sequence recouples the homonuclear dipolar interaction under MAS by the chemical shift difference modulated with π pulses. Though the dipolar interaction under the RFDR pulse sequence depends on the chemical shift difference, the dipolar interaction is recovered over a broad range of about $2/\tau_R$. Since the duty factor for the RF irradiation is small, the magnetization transfer with the RFDR pulse sequence is less susceptible to the relaxation due to CH dipolar interactions. This RFDR sequence has been applied to two-dimensional correlation NMR experiments for the signal assignments along the ^{13}C–^{13}C bonds and the measurements of internuclear distances (*33–36*).

We propose new π pulse trains referred to as compound RFDR (CRFDR) pulse sequences. The CRFDR pulse sequences reduce the γ dependence of the recoupled homo-

[1] Present address: Department of Chemical Sciences, Tata Institute of Fundamental Research, Homi Bhabha Road, Mumbai 400 005, India.

1090-7807/00 $35.00

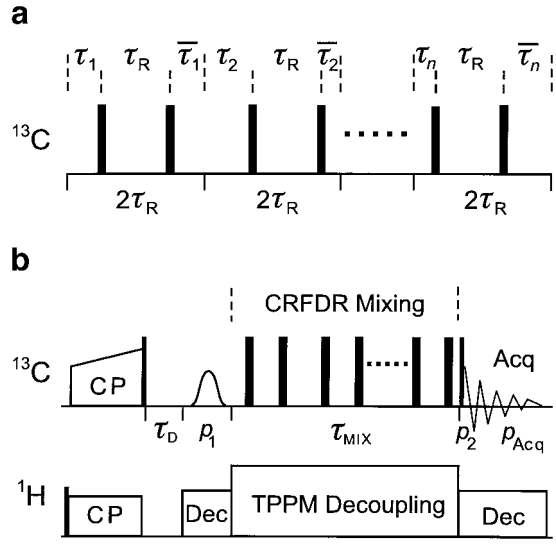

FIG. 1. (a) CRFDRn pulse sequence consisting of RFDR units, τ_i–π–τ_R–π–$\bar{\tau}_i$. (b) Pulse sequence for the measurement of the magnetization transfer under the CRFDR pulse sequence. The initial ^{13}C longitudinal magnetization is prepared by cross polarization followed by the 90° pulse. The Gaussian 90° pulse at the middle of the $^{13}C^{\alpha}$ and $^{13}C^{\beta}$ resonance frequencies cancels both signals. Thus the carboxyl ^{13}C z magnetization is prepared at the beginning of the mixing period under the CRFDR pulse sequence. The thin and thick dark pulses represent $\pi/2$ and π pulses, respectively. The RF phases are $p_1 = y\bar{y}$, and $p_2 = p_{Acq} = xx\bar{x}\bar{x}yy\bar{y}\bar{y}$, where $\bar{x}$ and $\bar{y}$ signify $-x$ and $-\bar{y}$. The other pulses have constant phases.

nuclear dipolar interaction under the RFDR pulse sequence. The recoupled dipolar interaction under CRFDR enhances the magnetization transfer efficiency of RFDR, similarly to HORROR and its derivatives. This paper presents a theory of the CRFDR pulse sequences based on the average Hamiltonian. Effects of chemical shift anisotropies and the other ^{13}C dipolar interactions on the CRFDR mixing were also studied. We demonstrate the enhanced magnetization transfer in experiments for fully ^{13}C-labeled alanine.

THEORY

Effective Hamiltonian for Compound RFDR Pulse Sequences

A compound RFDR pulse sequence (CRFDRn) consisting of n RFDR pulse units is shown in Fig. 1a. An RFDR unit is $2\tau_R$ in length so that the total pulse length of CRFDRn is $2n\tau_R$. We will derive the effective Hamiltonian for CRFDR to analyze its efficiency for the magnetization transfer.

The effective Hamiltonian for the ith RFDR unit with the delay τ_i is calculated from the coherent averaging theory for a two-spin system as follows (*26, 31, 37, 38*). The Hamiltonian for the system in the rotating frame comprises chemical shifts, a homonuclear dipole–dipole interaction, and the interaction with an RF field as

$$\mathcal{H} = \mathcal{H}_{INT} + \mathcal{H}_{RF}, \qquad [1]$$

$$\mathcal{H}_{INT}(t) = \delta_1(t)I_{1z} + \delta_2(t)I_{2z} + A_{20}^{LAB}(t)(3I_{1z}I_{2z} - \mathbf{I}_1\mathbf{I}_2)/\sqrt{6}, \qquad [2]$$

$$\mathcal{H}_{RF}(t) = -\boldsymbol{\omega}_1(t)(\mathbf{I}_1 + \mathbf{I}_2). \qquad [3]$$

Here δ_1 and δ_2 are chemical shifts, and the rotation frequency $\boldsymbol{\omega}_1$ is due to the RF field and offset. The tensor element of the dipolar interaction in the laboratory frame is

$$A_{20}^{LAB}(t) = -\sum_{l=-2}^{2} D_{l0}^{(2)}(\gamma + \omega_R t,\ \theta_{MAS},\ 0)d_{0l}^{(2)}(\beta)\sqrt{6}b, \qquad [4]$$

where $\omega_R = 2\pi/\tau_R$, $D_{l0}^{(2)}(\gamma + \omega_R t,\ \omega_{MAS},\ 0)$ is a Wigner rotation matrix element, $d_{0l}^{(2)}(\beta)$ is a reduced Wigner rotation matrix element, θ_{MAS} is the magic angle, β and γ are Euler angles for the coordinate transformation from the principal axis system of the dipolar interaction to the spinner frame, $b = \hbar\gamma_I^2 r^{-3}$, and γ_I and r are a gyromagnetic ratio and an internuclear distance. The internal Hamiltonian $\mathcal{H}_{INT}(t)$ in Eq. [2] is divided into the mutual commuting Hamiltonians,

$$\mathcal{H}_{\Delta}(t) = \tfrac{1}{2}(\delta_1(t) - \delta_2(t))(I_{1z} - I_{2z}) - A_{20}^{LAB}(t)(I_{1x}I_{2x} + I_{1y}I_{2y})/\sqrt{6}, \qquad [5]$$

$$\mathcal{H}_{\Sigma}(t) = \tfrac{1}{2}(\delta_1(t) + \delta_2(t))(I_{1z} + I_{2z}) + 2A_{20}^{LAB}(t)I_{1z}I_{2z}/\sqrt{6}. \qquad [6]$$

The propagator for the $2\tau_R$ period can be written with the Hamiltonians in the toggling frame driven by the π pulses in the RFDR unit,

$$U(2\tau_R) = \exp\left(-i\int_0^{2\tau_R}\mathcal{H}_{RF}(t)dt\right)\exp\left(-i\int_0^{2\tau_R}\tilde{\mathcal{H}}_{\Sigma}(t)dt\right) \times \mathrm{T}\exp\left(-i\int_0^{2\tau_R}\tilde{\mathcal{H}}_{\Delta}(t)dt\right), \qquad [7]$$

where

$$\tilde{\mathcal{H}}_{\Delta}(t) = \exp\left(i\int_0^t\mathcal{H}_{RF}(\tau)d\tau\right)\mathcal{H}_{\Delta}(t)\exp\left(-i\int_0^t\mathcal{H}_{RF}(\tau)d\tau\right) = \tfrac{1}{2}(\delta_1(t) - \delta_2(t))k(t)(I_{1z} - I_{2z}) - A_{20}^{LAB}(t) \times (I_{1x}I_{2x} + I_{1y}I_{2y})/\sqrt{6}, \qquad [8]$$

$$\tilde{\mathcal{H}}_{\Sigma}(t) = \tfrac{1}{2}(\delta_1(t) + \delta_2(t))k(t)(I_{1z} + I_{2z}) + 2A_{20}^{LAB}(t)I_{1z}I_{2z}/\sqrt{6}, \qquad [9]$$

T is the Dyson time-ordering operator, $k(t) = 1$ for $0 \le t < \tau_i$ and $\tau_i + \tau_R < t < 2\tau_R$, and $k(t) = -1$ for $\tau_i < t < \tau_i + \tau_R$. Since we are interested in the exchange of the z components given by $\mathrm{Tr}\{I_{2z}U(2j\tau_R)I_{1z}U^{-1}(2j\tau_R)\}$, where j is an integer, we can drop the first and second factors of the propagator in Eq. [7] and focus on the effect of $\tilde{\mathcal{H}}_{\Delta}(t)$.

The effective Hamiltonian for the dipolar interaction in Eq. [8] is calculated from the dipolar Hamiltonian in the frame rotated by the chemical shift difference $\tilde{\mathcal{H}}_{CS}(t)$,

$$\tilde{\tilde{\mathcal{H}}}_{DD}(t) = \exp\left(i \int_0^t \tilde{\mathcal{H}}_{CS}(\tau)d\tau \right)(-A_{20}^{LAB}(t) \times (I_{1x}I_{2x} + I_{1y}I_{2y})/\sqrt{6})\exp\left(-i \int_0^t \tilde{\mathcal{H}}_{CS}(\tau)d\tau \right), \quad [10]$$

where

$$\tilde{\mathcal{H}}_{CS}(t) = \tfrac{1}{2}(\delta_1(t) - \delta_2(t))k(t)(I_{1z} - I_{2z}). \quad [11]$$

The effective Hamiltonian is

$$\tilde{\tilde{\mathcal{H}}}_{DD}^{(0)} = \frac{1}{2\tau_R}\int_0^{2\tau_R} \tilde{\tilde{\mathcal{H}}}_{DD}(t)dt = C_1(\tau_i/\tau_R)\{(I_{1x}I_{2x} + I_{1y}I_{2y})\cos\phi_i - (I_{1y}I_{2x} - I_{1x}I_{2y})\sin\phi_i\}, \quad [12]$$

where $C_1(\tau_i/\tau_R)$ is an effective dipolar coupling strength, and ϕ_i depends on the chemical shifts, τ_i and τ_R. When we ignore the time dependence of δ_1 and δ_2 due to chemical shift anisotropies in Eq. [11],

$$C_1(\tau_i/\tau_R) = -\frac{2b}{\pi}\sum_{m=1}^{2}\left\{ d_{MAS}^{(m)}(\beta)\frac{\delta_{12}/\omega_R}{m^2 - (\delta_{12}/\omega_R)^2} \times \cos(m(\omega_R\tau_i + \gamma))\right\}\sin\frac{\delta_{12}\tau_R}{2}, \quad [13]$$

$$\phi_i = \delta_{12}(2\tau_i - \tau_R)/2, \quad [14]$$

$\delta_{12} = \delta_1 - \delta_2$, $d_{MAS}^{(1)}(\beta) = -(\sin 2\beta)/\sqrt{8}$, and $d_{MAS}^{(2)}(\beta) = (\sin^2\beta)/4$.

Equation [12] is the effective dipolar Hamiltonian generalized from the Hamiltonian at $\tau_i = \tau_R/2$ derived by Bennett *et al.* (*26, 31*). Equations [12] and [14] indicate that the delay τ_i modulates the phase ϕ_i for the zero-quantum (ZQ) spin operators, where $(I_{1x}I_{2x} + I_{1y}I_{2y}) = \{ZQ\}_x$ and $(I_{1y}I_{2x} - I_{1x}I_{2y}) = \{ZQ\}_y$ are the x and y components of the ZQ operators, respectively. Since $\{ZQ\}_x$, $\{ZQ\}_y$, and $\{ZQ\}_z = (I_{1z} - I_{2z})/2$ constitute a three-dimensional subspace as shown by $[\{ZQ\}_x, \{ZQ\}_y] = i\{ZQ\}_z$ and its cyclic permutations, the time dependence of $\{ZQ\}_z$ due to $\tilde{\tilde{\mathcal{H}}}_{DD}^{(0)}$ is independent of the phase angle ϕ_i for the ZQ operators in Eq. [12] (*39*). Therefore, the time dependence of $\{ZQ\}_z$, i.e., the transfer of the longitudinal magnetization, is determined only by $|C_1|$. This is analogous to that the z component of the magnetization rotated from the z direction by an RF pulse on resonance is independent of the RF phase and determined only by the flip angle.

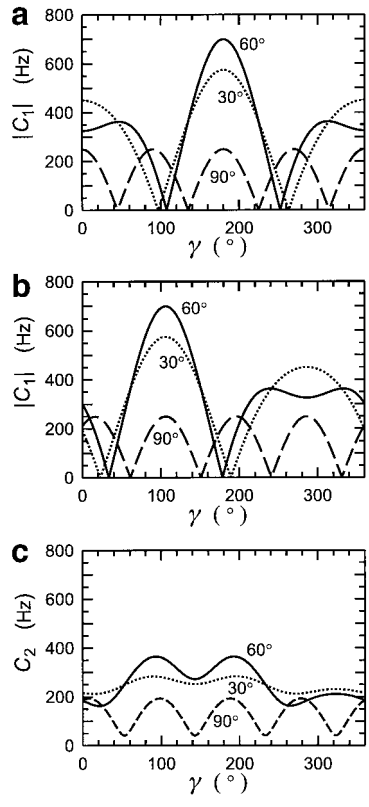

FIG. 2. Effective dipolar coupling strengths as a function of the initial spinner phase γ. (a) $|C_1(0.500)|$ of the RFDR unit calculated for the isotropic chemical shift difference of $\delta_{12}/2\pi = 13.0$ kHz. (b) $|C_1(0.705)|$ of the RFDR unit. (c) $C_2(0.500, 0.705)$ of the CRFDR2 pulse sequence. The effective coupling strengths are calculated for a ^{13}C–^{13}C internuclear distance of 1.55 Å. The coupling strengths at $\beta = 30°$, 60°, and 90° are shown by dotted, solid, and dashed lines, respectively. The sample spinning frequency is 8929 Hz.

The delay τ_i also modulates the γ dependence of the recoupled dipolar coupling strength $|C_1(\tau_i/\tau_R)|$ as indicated by $(\omega_R\tau_i + \gamma)$ in Eq. [13]. Figure 2a illustrates the recoupled dipolar coupling strength $|C_1(0.500)|$ at $\beta = 30°$, 60°, and 90° obtained for a ^{13}C two-spin system. When $\tau_i/\tau_R = 0.500$, $\phi_i = 0°$ and $\omega_R\tau_i = 180°$. Figure 2b shows $|C_1(0.705)|$ where $\phi_i = 108°$ and $\omega_R\tau_i = 254°$. Thus $|C_1|$ in Fig. 2a is shifted from that in Fig. 2b by 74° in γ.

The γ dependence of the effective dipolar interaction for RFDR in Eq. [12] can be reduced by averaging the effective

interactions over n RFDR units with different τ_i. The average Hamiltonian for CRFDRn (Fig. 1a) is given by

$$\tilde{\tilde{\mathcal{H}}}_{\mathrm{DD}}^{(0)} = \frac{1}{2n\tau_{\mathrm{R}}} \int_0^{2n\tau_{\mathrm{R}}} \tilde{\tilde{\mathcal{H}}}_{\mathrm{DD}}(t)dt$$

$$= C_n(\tau_i/\tau_{\mathrm{R}}, \tau_2/\tau_{\mathrm{R}}, \ldots, \tau_n/\tau_{\mathrm{R}})\{(I_{1x}I_{2x} + I_{1y}I_{2y}) \times \cos\phi_a - (I_{1y}I_{2x} - I_{1x}I_{2y})\sin\phi_a\}, \quad [15]$$

$$C_n(\tau_1/\tau_{\mathrm{R}}, \tau_2/\tau_{\mathrm{R}}, \ldots, \tau_n/\tau_{\mathrm{R}}) = \frac{1}{n}\sqrt{(\sum_{i=1}^{n} C_1(\tau_i/\tau_{\mathrm{R}})\cos\phi_i)^2 + (\sum_{i=1}^{n} C_1(\tau_i/\tau_{\mathrm{R}})\sin\phi_i)^2}. \quad [16]$$

Here, the average phase ϕ_a for the ZQ operators is dependent on τ_i and the orientation of the dipolar interaction, and $n > 1$. The transfer of the z magnetization under CRFDRn is determined by C_n in Eq. [16]. Figure 2c shows the γ dependence of the effective dipolar coupling strength $C_2(0.500, 0.705)$ for CRFDR2. This CRFDR2 pulse sequence is composed of the RFDR units giving $|C_1(0.500)|$ and $|C_1(0.705)|$ shown in Figs. 2a and 2b. The γ dependence of the effective dipolar coupling under CRFDR2 is weaker than that under RFDR. For example, the effective coupling strength C_2 for CRFDR2 varies in a range from 163 to 365 Hz at $\beta = 60°$ while $|C_1|$ for RFDR varies in a range from 0 to 699 Hz.

Dipolar Spectra for CRFDR

The averaging of the dipolar coupling under CRFDR for the powder orientations is evaluated with the dipolar spectra shown in Fig. 3. Those dipolar spectra are given by the Fourier transformation of the time-dependent $\{\mathrm{ZQ}\}_z$ operator expressed by

$$f(2j\tau_{\mathrm{R}}) = \int_0^{2\pi}\int_0^{\pi}\int_0^{2\pi} \mathrm{Tr}\{((I_{1z} - I_{2z})/2)U(2j\tau_{\mathrm{R}}) \times ((I_{1z} - I_{2z})/2)U^{-1}(2j\tau_{\mathrm{R}})\}\sin\beta\, d\alpha d\beta d\gamma, \quad [17]$$

where j is an integer, and α, β, and γ are Euler angles for generating the powder distribution. The signal calculated for CRFDR2 is split clearly into a doublet, while that for RFDR is not clearly, and has a considerable intensity at 0 Hz. These splittings of the dipolar spectra can be characterized by the average dipolar coupling $\langle\nu_{\mathrm{D}}\rangle$ and the linewidth $\Delta\nu_{\mathrm{D}}$ normalized by $\langle\nu_{\mathrm{D}}\rangle$. Here,

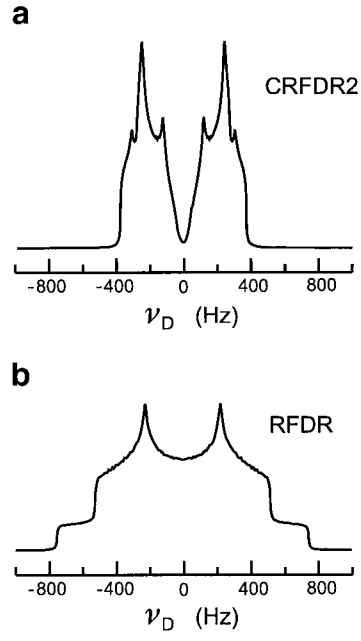

FIG. 3. Dipolar powder spectra for CRFDR2 (a) and RFDR (b) simulated for the ^{13}C two-spin system with a resonance frequency difference of 12.7 kHz. The other parameters are the same as those described in the legend to Fig. 2.

$$\langle\nu_{\mathrm{D}}\rangle = \int_0^{\infty} \nu_D I(\nu_D)d\nu_{\mathrm{D}} / \int_0^{\infty} I(\nu_{\mathrm{D}})d\nu_{\mathrm{D}}, \quad [18]$$

and $I(\nu_{\mathrm{D}})$ is the spectral intensity. The normalized linewidth is calculated from the root-mean-squared deviation of ν_{D} from $\langle\nu_{\mathrm{D}}\rangle$ as

$$\Delta\nu_{\mathrm{D}} = \sqrt{\int_0^{\infty} (\nu_{\mathrm{D}} - \langle\nu_{\mathrm{D}}\rangle)^2 I(\nu_{\mathrm{D}})d\nu_{\mathrm{D}} / \int_0^{\infty} I(\nu_{\mathrm{D}})d\nu_{\mathrm{D}}}/\langle\nu_{\mathrm{D}}\rangle. \quad [19]$$

The average and the linewidth give measures of the dipolar coupling strength and the broadening of the doublet due to the orientation dependence. The average dipolar couplings for CRFDR2 and RFDR are 217 and 290 Hz, respectively, at the ^{13}C–^{13}C internuclear distance of 1.55 Å. The average dipolar coupling $\langle\nu_{\mathrm{D}}\rangle$ for the static two-spin system without chemical shift difference is 786 Hz. Thus the effective dipolar interaction under CRFDR2 is scaled by a factor of 0.75 relative to that under RFDR, and scaled by 0.28 relative to that under the static condition. The normalized linewidth $\Delta\nu_{\mathrm{D}}$ for CRFDR, 0.41, is smaller than that for RFDR, 0.62. These $\Delta\nu_{\mathrm{D}}$ values confirm that CRFDR decreases the γ dependence of the effective coupling for RFDR as shown in Fig. 2.

TABLE 1
Delays in the CRFDR*n* Pulse Sequences and Averages of the Transferred Magnetization

	τ_2	τ_3	τ_4	$\overline{M_z}^a$
RFDR				0.52
CRFDR2	0.705			0.68
CRFDR3	0.330	0.205		0.68
CRFDR4	0.741	0.670	0.911	0.69
CRFDR4-1	0.616	0.348	0.750	0.69
CRFDR4-2	0.161	0.321	0.321	0.69

[a] The averages of the magnetization are given by the objective function in Eq. [20].

Optimization of CRFDR for Efficient Magnetization Transfer

The delays τ_i for the CRFDR pulse sequences are determined by maximizing the transferred magnetization in a range from ω_R to $5\omega_R/3$ in resonance frequency difference. The objective function for this maximization is

$$T(\tau_2, \ldots, \tau_n) = \max\{\overline{M_z}(\tau_{MIX}, \tau_1, \tau_2, \ldots, \tau_n); \tau_{MIX} \leq 3 \text{ ms}\}, \quad [20]$$

where

$$\overline{M_z}(\tau_{MIX}, \tau_1, \tau_2, \ldots, \tau_n) = \frac{3}{8\pi\omega_R} \int_{\omega_R}^{5\omega_R/3} \int_0^{2\pi} \int_0^{\pi} \mathrm{Tr}\{I_{2z} U(\tau_{MIX}) \times I_{1z} U^{-1}(\tau_{MIX})\} \sin\beta d\beta d\gamma d\delta_{12}. \quad [21]$$

Since τ_1 is fixed at $\tau_R/2$, the number of the delays τ_i determined for CRFDR*n* is $n - 1$. The CRFDR2, 3, and 4 pulse sequences were optimized with grid search in the range $0 < \tau_i < \tau_R$ for the two-spin system which has the ^{13}C–^{13}C dipolar coupling at the internuclear distance of 1.55 Å and isotropic chemical shifts. Table 1 shows the delays determined and the transferred magnetization averaged over the bandwidth. The transfer efficiency of CRFDR, i.e., the transferred magnetization averaged, is almost 70%. The transfer efficiency depends on the bandwidth where the transferred magnetization is evaluated. For example, the efficiencies of RFDR, CRFDR2, and CRFDR4 are 51, 65, and 68%, respectively, for the range from $0.6\omega_R$ to $1.6\omega_R$. These efficiencies should be compared with those in Table 1 evaluated for the range from ω_R to $5\omega_R/3$.

The weak orientational dependence for CRFDR as shown in Figs. 2 and 3 provides higher transfer efficiencies. Figure 4a showing the magnetization transfer indicates that the maximum magnetization transferred with the CRFDR pulse sequences is about 33% greater than that with the RFDR pulse sequence. The mixing time at the maximum transferred magnetization for CRFDR is longer than that for RFDR. This corresponds to the smaller average dipolar coupling $\langle \nu_D \rangle$ for CRFDR. The effective Hamiltonian $\tilde{\bar{\mathcal{H}}}^{(0)}_{DD}$ for CRFDR2 gives the transferred magnetization that agrees with the exact numerical calculation. This is shown in Fig. 4a by the agreement between the squares and the solid line, respectively, representing the results from $\tilde{\bar{\mathcal{H}}}^{(0)}_{DD}$ and the exact numerical calculation. Figure 4b exhibits the transferred magnetization depending on the resonance frequency difference. The magnetization transferred with CRFDR is larger than that with RFDR all over the frequency range.

We have found a number of delay sets, i.e., CRFDR pulse sequences, which give comparable maxima in the objective function value. This is partly due to the symmetry in the effective dipolar coupling strength C_n with respect to delays as follows. The dipolar coupling strength C_n given in the zeroth-order average Hamiltonian is not affected by the exchange of RFDR units within a CRFDR pulse sequence. The CRFDR*n* pulse sequence with $\tau_i = \tau'_i$ and that with $\tau_i = \tau_R - \tau'_i$ for $i =$ 1 to n give the same magnetization transfer for the powder,

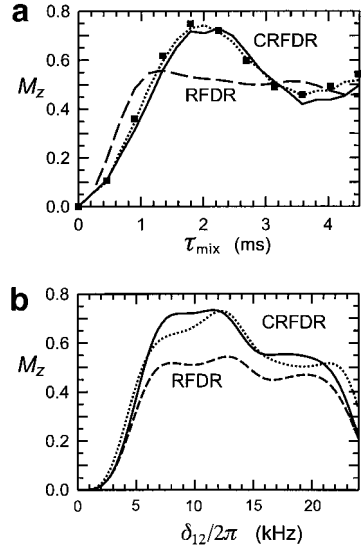

FIG. 4. Calculated magnetization transfer with the CRFDR4, CRFDR2, and RFDR pulse sequences for the two-spin system with a resonance frequency difference of 12.7 kHz. (a) The longitudinal magnetization transferred as a function of the mixing time with the CRFDR4, CRFDR2, and RFDR pulse sequences, respectively, shown by solid, dotted, and dashed lines. These z components were obtained by the exact numerical calculation for the powder. The transfer for CRFDR2 (squares) was computed from the zeroth-order average Hamiltonian theory. The maxima of the magnetization transferred with CRFDR4, CRFDR2, and RFDR are 0.73, 0.74, and 0.57, respectively. (b) The longitudinal magnetization transferred with CRFDR4 (solid), CRFDR2 (dotted), and RFDR (dashed) as a function of resonance frequency difference at mixing times that maximize the objective function Eq. [20]. The mixing times for CRFDR4, CRFDR2, and RFDR are 1.79, 1.79, and 1.12 ms, respectively. The other parameters are the same as those described in the legend to Fig. 2. The vertical axis indicates the magnetization normalized by the initial magnetization.

because the dipolar coupling strength C_n in Eq. [16] for the former CRFDRn at $\tau_i = \tau_i'$ and $\gamma = \gamma'$ is the same as that for the latter at $\tau_i = \tau_R - \tau_i'$ and at $\gamma = -\gamma'$. The CRFDR pulse sequence with $\tau_i = \tau_i'$ and that with $\tau_i = \tau_i' + \Delta\tau$ give the same dipolar spectrum, because the Hamiltonian for the RFDR units in Eq. [13] at $\tau_i = \tau_i'$ and $\gamma = \gamma'$ and that at $\tau_i = \tau_i' + \Delta\tau$ and $\gamma = \gamma' - \omega_R\,\Delta\tau$ have the same dipolar coupling strength $|C_1|$. Owing to these symmetries, the fix of τ_1 in the optimization would not much reduce the parameter space searched in this optimization.

APPLICATIONS OF THE CRFDR PULSE SEQUENCES

Effects of Chemical Shift Anisotropy

The RFDR pulse sequence recouples the dipolar interaction also under chemical shift anisotropy (*32*). This recovery of the dipolar interaction is due to the difference between time-dependent resonance frequencies as shown in Eqs. [10] and [12] for $\tilde{\tilde{\mathcal{H}}}_{DD}^{(0)}$. To evaluate the recoupling only by chemical shift anisotropies, we have calculated the dipolar spectra for the two-spin system having chemical shifts of spins corresponding to carboxyl carbons at a ^{13}C resonance frequency of about 100 MHz. Figure 5 shows the dipolar spectra obtained for CRFDR2 and RFDR from the exact calculation of the time-dependent $\{ZQ\}_z$ given by Eq. [17]. The average Hamiltonian $\tilde{\tilde{\mathcal{H}}}_{DD}^{(0)}$ in Eq. [12] also yields almost the same dipolar spectrum as shown in Fig. 5a for CRFDR2. The dipolar interaction recoupled by the chemical shift anisotropy shown in Fig. 5a is 183 Hz in $\langle\nu_D\rangle$. This average dipolar coupling is comparable to that recoupled by the isotropic chemical shift difference, 217 Hz, shown in Fig. 3a. The dipolar spectra depend on the relative orientations of the dipolar coupling and chemical shift anisotropies. Figures 5 (a, b) and (c, d) are calculated for the spin systems differing by 45° only in the orientation of the dipolar tensor relative to the shielding tensors. The average dipolar couplings obtained for Figs. 5c and 5d are less than half of those for Figs. 5a and 5b, respectively.

The CRFDR pulse sequences modify the recovery due to chemical shift anisotropies as well as that due to isotropic chemical shifts. The dipolar spectra recoupled by chemical shift anisotropies with the CRFDR2 and RFDR pulse sequences are shown in Figs. 5 (a, c) and (b, d), respectively. The dipolar splittings for CRFDR2 are more conspicuous than those for RFDR. These splittings are quantified by the normalized linewidth $\Delta\nu_D$, whose values are given in the legend to Fig. 5. The linewidths $\Delta\nu_D$ for CRFDR2 are smaller than those for RFDR by about 8%. This reduction in the linewidth by CRFDR under chemical shift anisotropies, however, is much smaller than that under isotropic chemical shifts calculated for Fig. 3, 35%.

When a pair of ^{13}C spins is separated by a chemical shift difference on the order of a high spinning frequency such as 15 kHz, one of the carbon spins generally has a large chemical shift anisotropy as a carbonyl or aromatic carbon has. We show the combined effects of isotropic and anisotropic chemical shift differences by simulations for the two-spin system composed of the carboxyl and C^α carbons in alanine (*40*) at a static magnetic field of 9.4 T. The carboxyl and C^α carbons have chemical shift anisotropies $|\sigma_{11} - \sigma_{33}| = 13.6$ and 3.4 kHz, respectively, and the isotropic chemical shift difference between them is 12.7 kHz. The calculated dipolar spectrum for CRFDR2 is shown in Fig. 6a. This dipolar spectrum is broader than that calculated without the anisotropies shown in Fig. 3a. The shielding anisotropies increase the normalized linewidth $\Delta\nu_D$ from 0.41 for Fig. 3a to 0.52 for Fig. 6a. This broadening in the frequency domain corresponds to the reduction of the maximum transferred magnetization in the time domain. The maxima of the transferred magnetization for the spin system with the shielding anisotropies are 0.68, 0.64, and 0.53 for CRFDR4, CRFDR2, and RFDR, respectively, as shown in Fig. 6b. These maxima are smaller than those for the system without the shielding anisotropies shown in Fig. 4a by about 10%. It should be noted that the maxima of the transferred magnetization under CRFDR4 and 2 are still larger than the maxi-

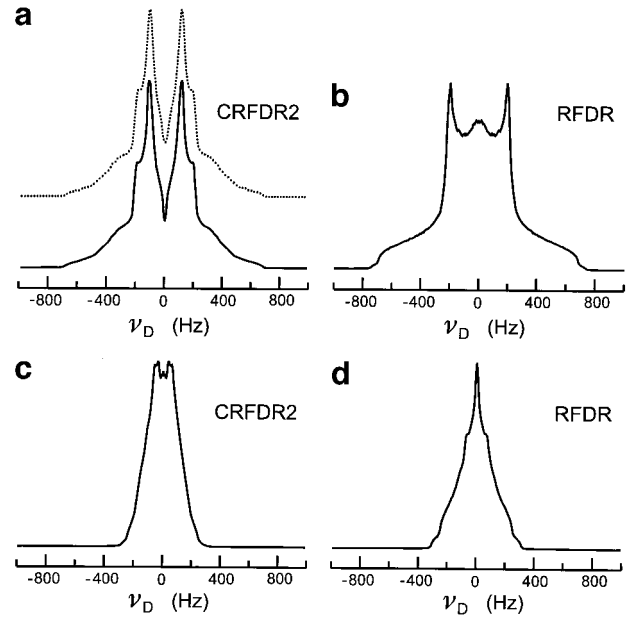

FIG. 5. Dipolar spectra due to chemical shift anisotropies in the two-spin systems for CRFDR2 (a, c) and RFDR (b, d). The spectrum for CRFDR2 obtained from the zeroth-order average Hamiltonian is shown by the dotted line. The principal values of the chemical shift tensors are −7.5, 0.0, and 7.5 kHz for the two spins. Euler angles for transforming the chemical shift tensors from the principal axis system to the molecular frame are (0°, 90°, 0°) and (0, 0°, 0°). Euler angles for the coordinate transformation of the dipolar tensor are (0°, 45°, 0°) for (a, b) and (0°, 0°, 0°) for (c, d). The ^{13}C–^{13}C distance is 1.55 Å. The sample spinning frequency is 8929 Hz. The average dipolar coupling $\langle\nu_D\rangle$ and the normalized linewidth $\Delta\nu_D$ are (182 Hz, 0.73), (210 Hz, 0.79), (85 Hz, 0.74), and (96 Hz, 0.80) for a, b, c, and d, respectively.

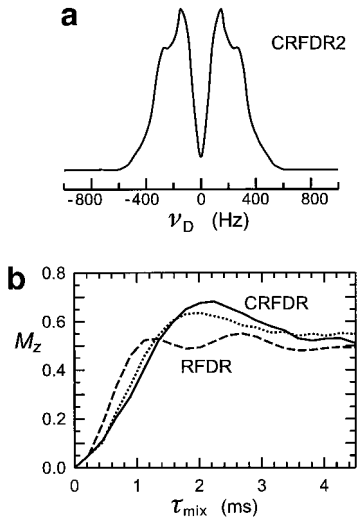

FIG. 6. Dipolar spectrum for CRFDR2 (a) and magnetization transfer (b) calculated for the two-spin system composed of $^{13}C^{\alpha}$ and ^{13}CO with the isotropic and anisotropic chemical shifts for alanine. (a) The average dipolar coupling $\langle \nu_D \rangle$ is 213 Hz. (b) The z components of the magnetization transferred from ^{13}CO to $^{13}C^{\alpha}$ with the pulse sequences CRFDR4, CRFDR2, and RFDR are shown by solid, dotted, and dashed lines, respectively. The other parameters are the same as those for Fig. 3.

mum under the RFDR sequence by about 25% even under the influence of the chemical shift anisotropies.

Experiments and Simulations for the ^{13}C Three-Spin System of Alanine

The magnetization transfer from ^{13}CO to $^{13}C^{\alpha}$ was calculated for the three-spin system composed of ^{13}CO, $^{13}C^{\alpha}$, and $^{13}C^{\beta}$ in alanine. The results are shown by solid lines in Fig. 7. We have used a finite RF amplitude of 85 kHz and the phase cycle xy-16 for the π pulses (*41*) only in the simulations for the three-spin system. The maxima of the transferred magnetization with CRFDR4, CRFDR2, and RFDR are 0.59, 0.56, and 0.49, which are about 10% smaller than those for the two-spin system with the shielding anisotropies shown in Fig. 6b. This reduction is mainly due to the ^{13}C dipolar interactions for $^{13}C^{\beta}$ and finite RF amplitude effects. In the three-spin system the magnetization is also transferred to $^{13}C^{\beta}$. Simulations for the magnetization transfer for the three-spin system with the infinite RF amplitude indicate that about a quarter of the reduction is attributed to the finite RF amplitude.

Experimental spectra for fully ^{13}C-labeled alanine at the mixing times giving the maximum transferred magnetization are shown in Fig. 8. The mixing-time dependence of the experimental transferred magnetization is indicated by circles in Fig. 7. The maxima of the magnetization transferred with the CRFDR4 and CRFDR2 sequences are about 15 and 8% larger than that with RFDR, respectively. These percentages should be compared with the enhancements of 20 and 14% by CRFDR4 and CRFDR2 in the simulations for the three-spin system. The CH dipolar interactions under decoupling fields and experimental imperfections such as RF field inhomogeneity would reduce the experimental signal intensities from the simulated ones as shown in Fig. 7. The higher transfer efficiencies for CRFDR are reflected in the lower carboxyl ^{13}C signal intensities in the spectra for CRFDR. Even though the mixing time used for CRFDR is about 1.7 times longer than that for RFDR, the $^{13}C^{\beta}$ intensities for the CRFDR pulse sequences are small and near to that for RFDR as shown in Fig. 8. Thus the magnetization transfer allows us to distinguish between the nearest and the next nearest ^{13}C spins. The CRFDR pulse sequences are optimized for the magnetization transfer in the two-spin systems, but this does not lead to the enhancement of the transferred magnetization from ^{13}CO to $^{13}C^{\beta}$ in the three-spin system of alanine. This is shown by the $^{13}C^{\beta}$ signal intensity that is smaller for CRFDR4 than for CRFDR2 and RFDR in the experiments (Fig. 8) and also in simulations (not shown).

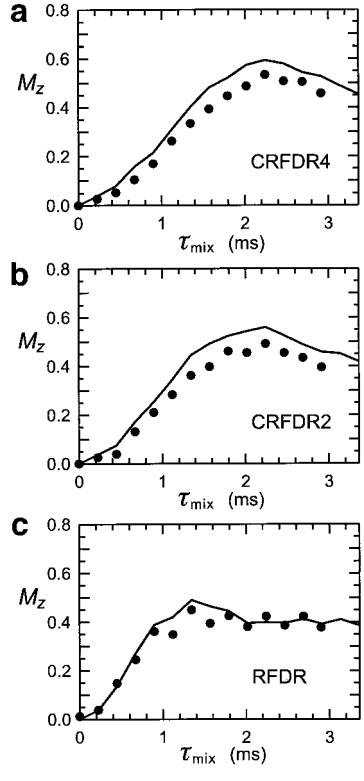

FIG. 7. Experimental (circles) and calculated (solid lines) magnetization transfer for triply ^{13}C-labeled alanine. The magnetization transferred from ^{13}CO to $^{13}C^{\alpha}$ with CRFDR4 (a), CRFDR2 (b), and RFDR (c) is shown as a function of the mixing time τ_{MIX}. The experimental C^{α} magnetization was obtained from the signal intensities with correction for the abundance of the ^{13}C pairs. The distance between the carboxyl and α carbons is 1.59 Å which is longer than that for Fig. 5 to fit the calculated to experimental magnetization. The maxima of the magnetization transferred with CRFDR4, CRFDR2, and RFDR in the experiments are 0.53, 0.49, and 0.45, respectively.

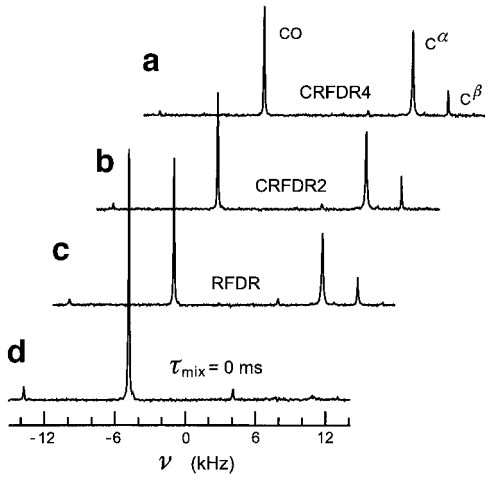

FIG. 8. Experimental ^{13}C spectra of fully ^{13}C-labeled alanine for the magnetization transfer. The spectra were obtained with the pulse sequences shown in Fig. 1b. The mixing pulse sequences are CRFDR4 (a), CRFDR2 (b), and RFDR (c) with $\tau_{MIX} = 2.24$, 2.24, and 1.34 ms, respectively. The reference spectrum (d) at $\tau_{MIX} = 0$ ms is also shown. All the spectra are displayed on the same vertical scale. The horizontal axis indicates the offset from the carrier frequency.

DISCUSSION

The *xy*-16 supercycle makes a π pulse train tolerant to off-resonance effects and RF field inhomogeneity (*41*). We have used *xy*-16 in the magnetization transfer experiments for CRFDR2 and CRFDR4. This supercycle combined with the CRFDR pulse sequences, however, is not so effective for suppressing off-resonance effects as that with RFDR. The RFDR pulse sequence has intervals of τ_R between π pulses. The CRFDR*n* pulse sequence has different intervals τ_R, $\bar{\tau}_{i-1} + \tau_i$, and $\bar{\tau}_n + \tau_1$, where $i = 2$ to n, as shown in Fig. 1a. While the *xy*-16 π pulse train with constant intervals has been shown to cancel off-resonance effects (*41, 42*), that with different intervals is generally not guaranteed to cancel them. Thus, when the RF field strength was decreased from 85 to 50 kHz, the ratio of the maximum transferred magnetization with CRFDR4 to that with RFDR decreased from 1.20 to 1.13 in the simulation for the three-spin system.

The suppression of off-resonance effects by the supercycle depends on the period of CRFDR*n*. The interference between the off-resonance effects and the RF pulses under CRFDR*n* with *xy*-16 was conspicuous at $n = 3$. The magnetization transferred from ^{13}CO to $^{13}C^{\alpha}$ in the three-spin system calculated for the CRFDR3 with the supercycle $(0, 2\pi/3)$-24, 0.56, was larger than that with *xy*-16, 0.47. Here the phase cycle of π pulses in $(0, 2\pi/3)$-24 is $(0, 2\pi/3)_3$ $(2\pi/3, 0)_3$ $(\pi, 4\pi/3)_3$ $(4\pi/3, \pi)_3$, and this supercycle has the subcycles containing six π pulses. Since CRFDR3 has six π pulses, CRFDR3 can be applied synchronously with the $(0, 2\pi/3)$-24 supercycle but not with *xy*-16. Therefore, the pulse imperfections of CRFDR3 in a subcyle of $(0, 2\pi/3)$-24 would be compensated by the imperfections in another subcycle. The subcycles of *xy*-16 composed of four or eight π pulses, however, include different portions of the CRFDR3 pulse sequence, so that the subcycles would not have imperfections that can be canceled in the supercycle. The best experimental magnetization transferred with CRFDR3 for fully ^{13}C-labeled alanine, 0.48, was obtained also with the $(0, 2\pi/3)$-24 supercycle. This transferred magnetization is about 6% larger than that with RFDR.

We have determined the delays τ_i in the CRFDR pulse sequences by maximizing the magnetization transfer in the two-spin systems with a dipolar interaction and isotropic chemical shift differences in a range. The optimal delays depend on the conditions at the maximization. Since the recovery of the dipolar interaction relies on the resonance frequency difference, the delays are dependent on the range of the frequency difference for the objective function. However, the delays would not be affected by the strength of the dipolar coupling, because the dipolar coupling constant only scales the effective dipole Hamiltonian according to the zeroth-order average Hamiltonian. The pulse sequences optimized for the two-spin system have superior performance also for the three-spin system with chemical shift anisotropy, because the shielding anisotropies and the presence of the third spin generally diminish the magnetization transferred with CRFDR by about 0.15 in the normalized magnetization. However, it may still be possible to improve the magnetization transfer slightly by optimizing the CRFDR pulses for chemical shift anisotropies. An example for differential sensitivity of the pulse sequences to chemical shift anisotropy is as follows. When the chemical shift anisotropies are added to the two-spin system for the simulation shown in Fig. 4a, the maxima of the transferred magnetization with CRFDR2 and CRFDR4 were decreased by 0.10 and 0.05, respectively. Thus, the reduction in the maximum for CRFDR2 is twice as large as that for CRFDR4.

The simulations without relaxation and the experiments have shown that the CRFDR pulse sequences enhance the maximum of the magnetization transferred under the RFDR pulse sequence. However, RFDR is more efficient in the initial time regime ($\tau_{MIX} < 1$ ms) as seen in Figs. 4 and 7. Therefore, under fast relaxation the maximum transferred magnetization would be larger for RFDR.

The pulse sequences CRFDR, C7, and the derivatives of C7 (*20–23*) are designed to reduce the γ dependence of the effective dipolar couplings over broadbands. This reduced dependence increases the efficiency for the magnetization transfer. While the RF phase rotation generates the DQ spin operators in the C7 pulse sequence, in the CRFDR pulse sequences the resonance frequency difference modulated by π pulses reintroduces the ZQ operators. Thus the recoupling by CRFDR depends on isotropic and anisotropic chemical shifts. The CRFDR pulse sequences do not completely eliminate the γ dependence as shown in Fig. 2, whereas C7 eliminates it. The pulse sequence CRFDR, however, enables the magnetization

transfer with the efficiency of about 69% for the two-spin system with isotropic shifts, which is comparable to the efficiency of 73% for C7. These similar efficiencies suggest that the further reduction of the γ dependence for CRFDR would only improve the efficiency slightly up to about 73%. Note that an efficiency higher than 73% is theoretically achievable by adiabatic magnetization transfer at the expense of a longer mixing time (*7*).

The magnetizations transferred by the ZQ and DQ spin operators are opposite in sign in the two-spin system. In a linear multispin system, the magnetization transferred by the DQ operators alternates in sign as it propagates along the chain of spins, while that by the ZQ operators does not. These complementary properties in the magnetization transfer make the combined use of the experiments for the ZQ and DQ dipolar couplings useful for identifying the magnetization transfer pathways and the estimate of distances in multispin systems.

CONCLUSIONS

We have designed the CRFDR pulse sequences composed of the RFDR pulse units. Owing to the time shifts of the π pulses in the units, the recoupled dipolar Hamiltonians in the RFDR units differ in the phase γ for the geometrical factor and the phase ϕ_i for the ZQ spin operators. The effective dipolar coupling for CRFDR is obtained from the zeroth-order Hamiltonian averaged over the whole CRFDR pulse sequence. The CRFDR pulse sequence, therefore, diminishes the γ dependence of the effective dipolar couplings under the RFDR pulse sequence, as shown in the dipolar spectra in Fig. 3. This reduced orientation dependence enhances the maximum of the transferred magnetization at the cost of a decrease in the effective dipolar coupling. The CRFDR pulse sequences also reduce the γ dependence of the dipolar interactions recoupled by chemical shift anisotropy. Though the chemical shift anisotropies of C^α and CO decrease the transferred magnetization in the two-spin system, the magnetization transferred with CRFDR is about 25% larger than that with RFDR.

Magnetization transfer experiments between CO and C^α in fully ^{13}C-labeled alanine were performed. The transferred magnetization with the CRFDR4 pulse sequence using the *xy*-16 supercycle was about 15% greater than that with RFDR. The CRFDR sequence can also be used for fully ^{13}C-labeled proteins. The magnetization transfer with CRFDR is efficient at resonance frequency differences comparable to the sample spinning rate. Therefore, CRFDR is suitable for the magnetization transfer between spins having considerable resonance frequency differences such as the ^{13}CO and $^{13}C^\alpha$ spins at high sample spinning rates.

EXPERIMENTAL

NMR Experiments

The magnetization transfer experiments were performed for ^{13}C-labeled alanine with the pulse sequence shown in Fig. 1b as follows. The initial *z* magnetization for ^{13}C was prepared by ramped-amplitude cross polarization (*43*) from the proton magnetization with a contact time of 1.8 ms and the following $\pi/2$ pulse. The proton RF amplitude was 65 kHz for the $\pi/2$ pulse and 53 kHz for the cross polarization. The carbon-13 RF amplitude was varied from 50 to 65 kHz in the cross polarization. The residual transverse magnetization dephased during the delay $\tau_D = 2$ ms without CH dipolar decoupling. The $^{13}C^\alpha$ and $^{13}C^\beta$ magnetizations of alanine were selectively excited by the Gaussian 90° pulse consisting of 24 rectangular pulses of 2.1 μs with intervals of 12.9 μs. These transverse magnetizations were canceled by the phase alternation of the Gaussian pulse relative to the phase of the final 90° pulse. The ^{13}C π pulse widths were 5.9 μs. The proton RF amplitude of the TPPM sequence for the CH dipolar decoupling was 66 kHz during the detection period and about 140 kHz during the ^{13}C–^{13}C dipolar mixing period. The TPPM sequence comprises 170° pulses with RF phase shifts of 14° (*44*). The sample spinning frequency was 8929 Hz with a precision of about 10 Hz. The number of accumulations was 16. The spectral width was 80 kHz. An FID with 1024 data points was zero-filled to 4096 points and Fourier-transformed with an exponential line-broadening factor of 100 Hz. The recycle delay was 7 s. All the experiments were performed at room temperature on a Chemagnetics CMX-400 Infinity spectrometer with a broadband double-resonance probe for a 4-mm rotor under a static magnetic field of 9.4 T. The powdered sample was composed of natural-abundance L-alanine and 97% ^{13}C, ^{15}N-labeled L-alanine purchased from Shoko Co. Ltd. with the ratio 5:1.

Numerical Simulations

The time evolution of the spin system was calculated by the numerical integration of a time-dependent Hamiltonian including terms for the ^{13}C dipolar interaction and chemical shifts (*16*). A propagator for a 2π sample rotation was expressed as the product of about 130 propagators calculated on the assumption of the time independence during the short piecewise sections. The structural parameters for specifying the dipolar interactions and chemical shift anisotropies were taken from the single-crystal studies (*40, 45*) with a correction (*29*). The isotropic *J* couplings, $J = 35$ Hz for the $^{13}C^\alpha$–$^{13}C^\beta$ pair and 55 Hz for the $^{13}C^\alpha$–^{13}CO pair, were included only in the calculation for the three-spin system. The time-domain signals with 1024 points for about 2×10^5 orientations were summed up for a powder spectrum. The calculated signal was zero-filled to 2048 points and Fourier-transformed with a line-broadening factor of 8 Hz. The magnetization transfer and dipolar spectra

were calculated on an SGI Origin200 workstation having four R10000 processors.

ACKNOWLEDGMENTS

This research was partially supported by Grant-in-Aids for Scientific Research from the Ministry of Education and the Shimadzu Science Foundation.

REFERENCES

1. R. G. Griffin, Dipolar recoupling in MAS spectra of biological solids, *Nature Struct. Biol.* **5,** 508–512 (1998).
2. M. Baldus, D. G. Geurts, and B. H. Meier, Broadband dipolar recoupling in rotating solids: A numerical comparison of some pulse schemes, *Solid State NMR* **11,** 157–168 (1998).
3. A. E. Bennett, R. G. Griffin, and S. Vega, Recoupling of homo- and heteronuclear dipolar interactions in rotating solids, *NMR Basic Principles Prog.* **33,** 1–77 (1994).
4. T. Fujiwara, A. Ramamoorthy, K. Nagayama, K. Hioka, and T. Fujito, Dipolar HOHAHA under MAS conditions for solid-state NMR, *Chem. Phys. Lett.* **212,** 81–84 (1993).
5. B.-Q. Sun, P. R. Costa, D. Kocisko, P. T. Lansbury, Jr., and R. G. Griffin, Internuclear distance measurements in solid state nuclear magnetic resonance: Dipolar recoupling via rotor synchronized spin locking, *J. Chem. Phys.* **102,** 702–707 (1995).
6. M. Baldus and B. H. Meier, Broadband polarization transfer under magic-angle spinning: Application to total through-space-correlation NMR spectroscopy, *J. Magn. Reson.* **128,** 172–193 (1997).
7. R. Verel, M. Baldus, M. Nijman, J. W. M. van Os, and B. H. Meier, Adiabatic homonuclear polarization transfer in magic-angle spinning solid-state NMR, *Chem. Phys. Lett.* **280,** 31–39 (1997).
8. M. H. Levitt, D. P. Raleigh, F. Creuzet, and R. G. Griffin, Theory and simulations of homonuclear spin pair systems in rotating solids, *J. Chem. Phys.* **92,** 6347–6364 (1990).
9. R. Tycko and S. O. Smith, Symmetry principles in the design of pulse sequences for structural measurements in magic angle spinning nuclear magnetic resonance, *J. Chem. Phys.* **98,** 932–943 (1993).
10. D. M. Gregory, D. J. Mitchell, J. A. Stringer, S. Kiihne, J. C. Shiels. J. Callahan, M. A. Mehta, and G. P. Drobny, Windowless dipolar recoupling: The detection of weak dipolar couplings between spin $\frac{1}{2}$ nuclei with large chemical shift anisotropies, *Chem. Phys. Lett.* **246,** 654–663 (1995).
11. P. R. Costa, B. Sun, and R. G. Griffin, Rotational resonance tickling: Accurate internuclear distance measurement in solids, *J. Am. Chem. Soc.* **119,** 10821–10830 (1997).
12. S. R. Kiihne, K. B. Geahigan, N. A. Oyler, H. Zebroshki, M. A. Mehta, and G. P. Drobny, Distance measurements in multiply labeled crystalline cytidines by dipolar recoupling solid state NMR, *J. Phys. Chem. A* **103,** 3890–3903 (1999).
13. H. C. Jarrelll, D. Lu, and D. Siminovitch, ^{13}C–^{13}C correlations and internuclear distance measurements with 2D-MELODRAMA, *J. Am. Chem. Soc.* **120,** 10453–10462 (1998).
14. Y. Ishii, T. Terao, and M. Kainosho, Relayed anisotropy correlation NMR: Determination of dihedral angles in solids, *Chem. Phys. Lett.* **256,** 133–140 (1996).
15. T. Fujiwara, T. Shimomura, and H. Akutsu, Multidimensional solid-state nuclear magnetic resonance for correlating anisotropic interactions under magic-angle spinning conditions, *J. Magn. Reson.* **124,** 147–153 (1997).
16. T. Fujiwara, T. Shimomura, Y. Ohigashi, and H. Akutsu, Multidimensional solid-state nuclear magnetic resonance for determining the dihedral angle from the correlation of ^{13}C–^{1}H and ^{13}C–^{13}C dipolar interactions under magic-angle spinning conditions, *J. Chem. Phys.* **109,** 2380–2393 (1998).
17. T. Fujiwara, K. Sugase, M. Kainosho, A. Ono, A. (M.) Ono, and H. Akutsu, ^{13}C–^{13}C and ^{13}C–^{15}N dipolar correlation NMR of uniformly labeled organic solids for the complete assignment of their ^{13}C and ^{15}N signals: An application to adenosine, *J. Am. Chem. Soc.* **117,** 11351–11352 (1995).
18. B.-Q. Sun, C. M. Rienstra, P. R. Costa, J. R. Williamson, and R. G. Griffin, 3D ^{15}N–^{13}C–^{13}C chemical shift correlation spectroscopy in rotating solids, *J. Am. Chem. Soc.* **119,** 8540–8546 (1997).
19. S. K. Straus, T. Bremi, and R. R. Ernst, Experiments and strategies for the assignment of fully $^{13}C/^{15}N$-labelled polypeptides by solid state NMR, *J. Biomol. NMR* **12,** 39–50 (1998).
20. Y. K. Lee, N. D. Kurur, M. Helmel, O. G. Johannessen, N. C. Nielsen, and M. H. Levitt, Efficient dipolar recoupling in the NMR of rotating solids. A sevenfold symmetric radiofrequency pulse sequence, *Chem. Phys. Lett.* **242,** 304–309 (1995).
21. M. Hohwy, H. J. Jakobsen, M. Eden, M. H. Levitt, and N. C. Nielsen, Broadband dipolar recoupling in the nuclear magnetic resonance of rotating solids: A compensated C7 pulse sequence, *J. Chem. Phys.* **108,** 2686–2694 (1998).
22. C. M. Rienstra, M. E. Hatcher, L. J. Muller, B. Sun, S. W. Fesik, and R. G. Griffin, Efficient multispin homonuclear double-quantum recoupling for magic-angle spinning NMR: ^{13}C–^{13}C correlation spectroscopy of U-^{13}C-erythromycin A, *J. Am. Chem. Soc.* **120,** 10602–10612 (1998).
23. M. Hohwy, C. M. Rienstra, C. P. Jaroniec, and R. G. Griffin, Fivefold symmetric homonuclear dipolar recoupling in rotating solids: Application to double quantum spectroscopy, *J. Chem. Phys.* **110,** 7983–7992 (1999).
24. N. C. Nielsen, H. Bildsøe, H. J. Jakobsen, and M. H. Levitt, Double-quantum homonuclear rotary resonance: Efficient dipolar recovery in magic-angle spinning nuclear magnetic resonance, *J. Chem. Phys.* **101,** 1805–1812 (1994).
25. X. Feng, P. J. E. Verdegem, Y. K. Lee, D. Sandström, M. Edén, P. Bovee-Geurts, W. J. de Grip, J. Lugtenburg, H. J. M. de Groot, and M. H. Levitt, Direct determination of a molecular torsional angle in the membrane protein rhodopsin by solid-state NMR, *J. Am. Chem. Soc.* **119,** 6853–6857 (1997).
26. A. E. Bennett, J. H. Ok, R. G. Griffin, and S. Vega, Chemical shift correlation spectroscopy in rotating solids: Radio frequency-driven recoupling and longitudinal exchange, *J. Chem. Phys.* **96,** 8624–8627 (1992).
27. T. Gullion and S. Vega, A simple magic angle spinning NMR experiment for the detection of rotational echoes of dipolar coupled homonuclear spin pairs, *Chem. Phys. Lett.* **194,** 423–428 (1992).
28. D. K. Sodickson, M. H. Levitt, S. Vega, and R. G. Griffin, Broad band dipolar recoupling in the nuclear magnetic resonance of rotating solids, *J. Chem. Phys.* **98,** 6742–6748 (1993).
29. W. Zhu, C. A. Klug, and J. Schaefer, Measurement of dipolar coupling within isolated spin-$\frac{1}{2}$ homonuclear pairs by CEDRA NMR, *J. Magn. Reson. A* **108,** 121–123 (1994).
30. O. Weintraub, S. Vega, Ch. Hoelger, and H. H. Limbach, Coherence transfer in dipolar-coupled homonuclear spin systems in solids rotating at the magic angle, *J. Magn. Reson. A* **110,** 12–18 (1994).
31. A. E. Bennett, C. M. Reinsert, J. M. Griffith, W. Hen, P. T. Lansbury,

Jr., and R. G. Griffin, Homonuclear radio frequency-driven recoupling in rotating solids, *J. Chem. Phys.* **108,** 9463–9479 (1998).

32. A. E. Bennett, D. P. Weliky, and R. Tycko, Quantitative conformational measurements in solid state NMR by constant-time homonuclear dipolar recoupling, *J. Am. Chem. Soc.* **120,** 4897–4898 (1998).

33. J. M. Griffiths, K. V. Lakshmi, A. E. Bennett, J. Raap, C. M. van der Wielen, J. Lugtenburg, J. Herzfeld, and R. G. Griffin, Dipolar correlation NMR spectroscopy of a membrane protein, *J. Am. Chem. Soc.* **116,** 10178–10181 (1994).

34. T. A. Egorova-Zachernyuk, B. van Rossum, G.-J. Boender, E. Franken, J. Ashurst, J. Raap, P. Gast, A. J. Hoff, H. Oschkinat, and H. J. M. de Groot, Characterization of pheophytin ground states in *Rhodobacter sphaeroides* R26 photosynthetic reaction centers from multispin pheophytin enrichment and 2-D ^{13}C MAS NMR dipolar correlation spectroscopy, *Biochemistry* **36,** 7513–7519 (1997).

35. M. T. Zell, B. E. Padden, D. J. W. Grant, M.-C. Chapeau, I. Prakash, and E. J. Munson, Two-dimensional high speed CP/MAS NMR spectroscopy of polymorphs. 1. Uniformly ^{13}C-labeled aspartame, *J. Am. Chem. Soc.* **121,** 1372–1378 (1999).

36. E. Zaborowski, H. Zimmermann, and S. Vega, Distance measurements between ^{13}C nuclei in singly labeled *p*-xylene/dianin's inclusion compound by 2D-RFDR, *J. Magn. Reson.* **136,** 47–53 (1999).

37. U. Haeberlen and J. S. Waugh, Coherent averaging effects in magnetic resonance, *Phys. Rev.* **175,** 453–467 (1968).

38. M. Mehring, "Principles of High Resolution NMR in Solids," 2nd ed., Springer-Verlag, Berlin (1983).

39. M. Kadkhodaie, O. Rivas, M. Tan, A. Mohebbi, and A. J. Shaka, Broadband homonuclear cross polarization using flip-flop spectroscopy, *J. Magn. Reson.* **91,** 437–443 (1991).

40. A. Naito, S. Ganapathy, K. Akasaka, and C. A. McDowell, Chemical shielding tensor and ^{13}C–^{14}N dipolar splitting in single crystals of L-alanine, *J. Chem. Phys.* **74,** 3190–3197 (1981).

41. T. Gullion, D. B. Baker, and M. S. Conradi, New, compensated Carr–Purcell sequences, *J. Magn. Reson.* **89,** 479–484 (1990).

42. Y. Li and J. N. S. Evans, The importance of *XY*-8 phase cycling in the rotational-echo phase cycling double-resonance experiment with total sideband suppression, *J. Magn. Reson. A* **116,** 150–155 (1995).

43. G. Metz, X. Wu, and S. O. Smith, Ramped-amplitude cross polarization in magic-angle-spinning NMR, *J. Magn. Reson. A* **110,** 219–227 (1994).

44. A. E. Bennett, C. M. Rienstra, M. Auger, K. V. Lakshmi, and R. G. Griffin, Heteronuclear decoupling in rotating solids, *J. Chem. Phys.* **103,** 6951–6958 (1995).

45. M. S. Lehmann, T. F. Koetzle, and C. W. Hamilton, Precision neutron diffraction structure determination of protein and nucleic acid components. I. The crystal and molecular structure of the amino acid L-alanine, *J. Am. Chem. Soc.* **94,** 2657–2660 (1972).